J Mater Sci (2009) 44:875–881
DOI 10.1007/s10853-008-3193-x

High-porosity NiTi superelastic alloys fabricated by low-pressure sintering using titanium hydride as pore-forming agent

H. Li · B. Yuan · Y. Gao · C. Y. Chung · M. Zhu

Received: 26 July 2008 / Accepted: 12 December 2008 / Published online: 31 December 2008

Abstract Porous NiTi shape memory alloys (SMAs) were successfully fabricated by low-pressure sintering (LPS), and the pore features have been controlled by adjusting the processing parameters. The porous NiTi SMAs with high porosity (45%) and large pore size (200–350 μm) can be prepared by LPS using $TiH_{1.5}$ as pore-forming agent. These alloys exhibit isotropic pore structure with three-dimensional interconnected pores. The porous NiTi SMA produced by LPS exhibits superelasticity and mechanical properties superior to that by conventional sintering.

Introduction

Porous NiTi shape memory alloys (SMAs) have been employed successfully in many applications including bone tissue engineering [1], energy absorption [2], and hydrogen isotope separation [3] because they inherit most of the excellent properties from dense NiTi SMAs, such as good biocompatibility, unique shape memory effect, and superelasticity. Moreover, they also possess many benefits of common porous metals, such as low density, high surface area, and high permeability [1, 4]. Biomedical application is still the main driving force for the extensive research on porous NiTi SMAs. Presently, the principal objective is still focused at developing one simple and reliable method to precisely fabricate superelastic porous NiTi SMAs, which can meet the requirements, e.g., 30–70% porosity and 100–500-μm pore size in terms of pore feature, of hard-tissue replacement materials. Up to now, many porous NiTi SMAs with different pore structures have been developed by different powder metallurgy (PM) methods, including conventional sintering (CS) [5, 6], self-propagating high-temperature synthesis (SHS) [7, 8], spark plasma sintering (SPS) [9], traditional hot isostatic pressing (HIP) processes [10], and capsule-free hot isostatic pressing (CF-HIP) [11].

Although, porous NiTi SMAs fabricated by different processes exhibit different pore features and mechanical properties, none is able to satisfy all the requirements for the hard-tissue replacement materials. The CS method requires long duration of heating, and the pore shape and size cannot be controlled easily. Porous NiTi SMAs prepared by SHS show high porosity (about 40–50%) and large pore size (about 200–500 μm). Nevertheless, one of the difficulties of using SHS is to control the sintering process, and the porous NiTi SMAs prepared by SHS exhibit unsatisfactory mechanical properties and superelasticity. The SPS method produces porous NiTi SMA with small pore size and low porosity. Furthermore, the pre-alloyed NiTi powder is required for SPS. On the other hand, porous NiTi SMAs fabricated by CF-HIP exhibit good superelasticity and relatively low porosity (<40%) [11], whereas the HIP/CF-HIP processes require high pressure and high temperature, thus making the cost of the equipments and manufacturing highly prohibitive.

Recently, an effective technique was used to precisely fabricate porous NiTi SMAs with high porosity and large pore size, where the elements (Ni and Ti) or pre-alloy NiTi

H. Li · B. Yuan · Y. Gao · M. Zhu (✉)
School of Materials Science and Engineering, South China University of Technology, Guangzhou 510641, People's Republic of China
e-mail: memzhu@scut.edu.cn

C. Y. Chung
Department of Physics & Materials Science, City University of Hong Kong, Kowloon, Hong Kong

Table 1 Designation and nominal compositions of the green samples

Sample no.	Composition	Cold pressure (MPa)	Sintering method	Porosity (%)	Pore size (μm)
I	50.8at.%Ni + 49.2at.%Ti-1	400	LPS	15.1	≤50
II	50.8at.%Ni + 49.2at.%Ti-1	50	LPS	30.3	50–150
III	50.8at.%Ni + 49.2at.%Ti-2	50	LPS	45.6	200–350
IV	50.8at.%Ni + 49.2at.%Ti-1	50	CS	33.2	≤50

powders were mixed with pore-forming agent or space-holder powder: for example, NaF was used in HIP [12] and NH_4HCO_3 in CF-HIP [13]. This is due to the fact that the high pressure in the HIP can prevent the gas in green sample from escaping [14], and therefore, favor forming high porosity and large spherical pores. Low pressure sintering (LPS) is a common method of powder metallurgy. Although only a relatively low pressure (≤5 MPa) is applied during sintering in LPS, the low pressure can accelerate the pore formation. However, comparing with HIP or CF-HIP with which the pressure is higher than 100 MPa, the pressure in LPS is considerably low. Thus, it makes not only the fabricating cost cheaper, but also the operational process easier. It is known that TiH_2 is a common pore-forming agent used for preparing porous Ti and Al metals. However, Li et al. [15] reported that porous NiTi SMAs exhibit low porosity and smaller pore size when fabricated by CS using TiH_2 as pore-forming agent. The purpose of this study is to explore the possibility of fabricating porous NiTi SMAs with high porosity by LPS using titanium hydride as pore-forming agent, and to investigate their mechanical properties.

Experimental

Ni powders and two types of Ti powders denoted as Ti-1 and Ti-2 were used in this study. The Ni powders have particle size of 50 μm and purity ≥99.5% (Co ≤ 0.1%, C ≤ 0.05%, Ca ≤ 0.03%, S ≤ 0.03%, Cu ≤ 0.03%, Fe ≤ 0.03%, Mn ≤ 0.03%, Mg ≤ 0.015%), the Ti-1 powders have particle size of 50 μm and purity ≥99.5% (O ≤ 0.16%, N ≤ 0.1%,Fe ≤ 0.1%, C ≤ 0.05%, Cl ≤ 0.05%, Al ≤ 0.03%), and the Ti-2 powders have particles size of 50 μm and contain about 30% $TiH_{1.5}$ which comes from the incomplete dehydrogenated process during the production of Ti powders. The powder mixture with composition of Ti–50.8at.%Ni was blended in a UBM-4 mill for 4 h. The rotation speed of the mill is 150 rpm and the weight ratio of ball to powder is 4:1. The blended powder mixtures were pressed to cylindrical green samples at different pressures using a hydraulic press. The green samples were put into crucible and reactive sintered in the LPS chamber in a RUBISTAR 60/1600 Graphite furnace. Table 1 shows the serial number of samples, and the type of powders, press pressure, and sintering conditions used to prepare them. The LPS chamber was vacuum purged and backfilled with 99.995% high purity argon gas before increasing the LPS pressure. The temperature of the LPS chamber was then increased. The argon pressure and temperature reached 5 MPa and 1050 °C, respectively, at the same time. The argon pressure and temperature were maintained for 3 h to allow sufficient solid-state diffusion of the nickel and titanium atoms. The argon gas was released suddenly once the sintering was over. The sample IV is sintered at 1050 °C for 3 h under the vacuum environment, i.e., CS sintering. The specimens obtained by LPS and CS were subjected to aging treatment at 450 °C in a tube furnace under the protection of high purity argon gas for 0.5 h followed by ice-water quenching. The densities of specimens were measured by the Archimedes' principle. A LEICA microsystem imaging solutions (LEICA Qwin Standard) was used to analyze the pore size distribution. An OLYMPUS BH-2 microscope and an X'pert MPD Pro X-ray diffractometer with Cu–Ka radiation ($\lambda = 1.54056$ Å) were used to characterize the microstructure. A TA differential scanning calorimeter (DSC 2910) was used to determine the phase transformation temperatures. Both the heating and cooling rates employed were 5 °C/min. The samples were machined into cylindrical shape (length diameter: 12 × 6 mm^2) to characterize superelasticity, and then aged at 450 °C for 0.5 h. Compression tests were performed with an Instron 4206 material test system at an initial strain rate of 3.33×10^{-3} s^{-1}. The compressive strain is 4%. The tests were performed at 50 °C, because the reverse martensitic transformation finish temperatures (A_f) for all the samples are lower than 40 °C.

Results and discussion

Pore morphology and distribution

Macrographs of pore morphology and distribution of Sample III along transverse and longitudinal directions are shown in Fig. 1, respectively. It can be seen that pore morphology and distribution along both directions exhibit isotropic and uniform characteristics in porous NiTi SMAs

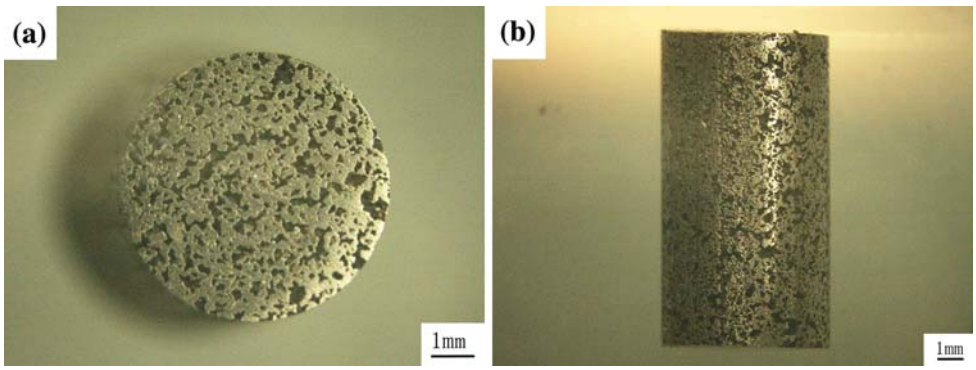

Fig. 1 Marographs of porous Ti–50.8at.%Ni SMAs sintered by LPS **a** Radial **b** Axial

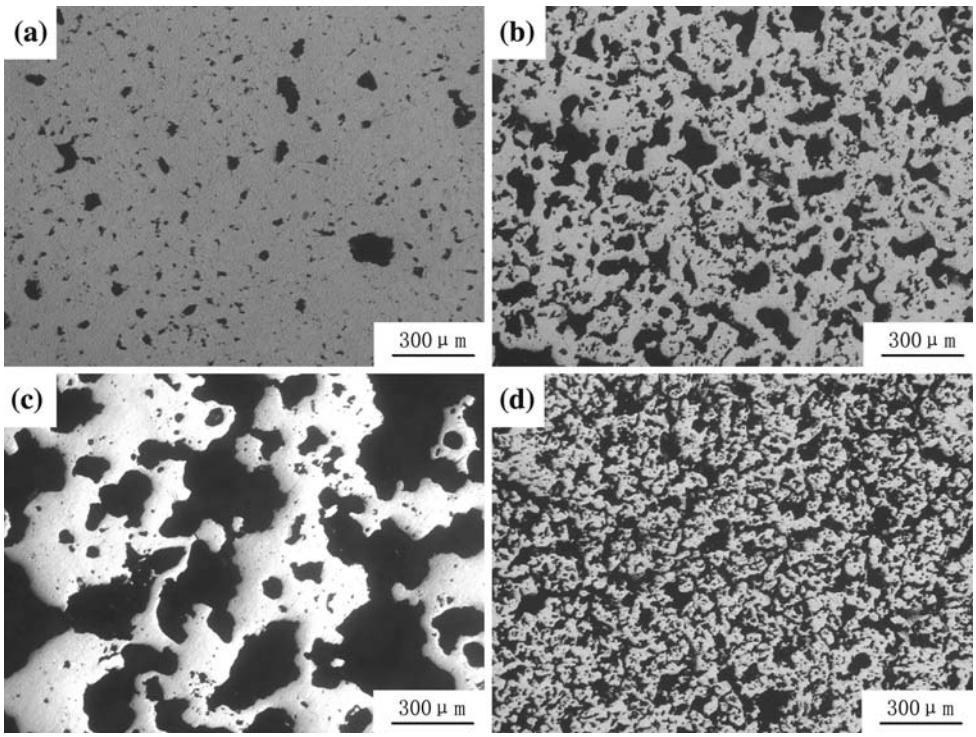

Fig. 2 Optical micrographs of porous Ti–50.8at.%Ni SMAs with different porosities sintered by LPS and CS: **a** sample I with 15.1% porosity, **b** sample II with 30. 3%, **c** sample III with 45.6%, and **d** sample IV with 33.2%

prepared by LPS. The other samples have the macroscopic morphology similar to that of sample III. Figure 2a–c, corresponding to the samples, I–III, shows the three optical micrographs of porous Ti–50.8at.%Ni SMAs fabricated by LPS using different parameters, which correspond to the three porosity ratios (P) of 15.1%, 30.3%, and 45.6%, respectively. It can be observed that most of pores in all the samples are near by spherical and isolated, and they exhibit a homogeneous pore distribution. It can be seen clearly that the connected pores and the pore size increase with increasing porosity ratios. Taking sample I and sample II as examples, the spherical pores in Fig. 2a are rarely interconnected and are of very small pore size <50 μm, whereas the connected pores increase with pore size in the range of 50–150 μm in the sample II with porosity of 30.3%, as shown in Fig. 2b. From Table 1, we can see that sample I has the same parameters as for sample II except for cold pressure. It is suggested that cold pressure is an effective control parameter to adjust the pore size and porosity of porous NiTi SMAs.

The pores in sample III, as presented in Fig. 2c, are obviously three-dimensional interconnected porous structure, and most of the pores are large spherical ones with the size in the range of 200–350 μm, which are suitable for bone tissue integration [16]. There are some small pores sparsely located around the large pore walls. These small pores are closed ones. The pore morphology and distribution of porous NiTi SMAs prepared by LPS and CF-HIP [11] are similar. However, the specimens that are prepared by CS have obviously different pore morphologies compared with LPS specimen. The sample IV with porosity ratio of 33.2% was prepared by CS. Figure 2d shows the morphology of the sample IV, and it can be seen that the pore shape is irregular and most pores are small (<50 μm). This suggests that by

means of the LPS process the morphology of porous NiTi SMAs can be controlled through adjusting the sintering pressure. The pore features changed slightly compared to those obtained when fabricated by CF-HIP.

By comparing Fig. 2c with 2b, it can be found that the pores become larger and the porosity increases obviously under the same cold pressure and sintering method. These results indicated that the $TiH_{1.5}$ plays a key role in pore forming because of the only difference in the compositions between Ti-1 and Ti-2 powder (containing 30% $TiH_{1.5}$) that were adopted in the samples II and III, respectively.

The green samples would undergo further compression after the cabin was filled with low-pressure argon gas. The low-pressure argon gas would penetrate into part of cavities and expel the air in cavities. It is known that titanium hydride (TiH_x) would decompose to Ti and H_2 when the temperature is above 480 °C. As the temperature was higher than 480 °C, $TiH_{1.5}$ started to decompose. Because of the argon gas pressure, the decomposed hydrogen got attached to the surface of the Ti particles initially. When the temperature continues to rise, the decomposed hydrogen begins to congregate together. The gathered hydrogen gas would form some bubbles. The hydrogen bubbles act as an underprop in cavities thus preventing the densification during sintering. Some of the original open, interconnected, and closed pores are retained because of the entrapment of the hydrogen gas bubbles.

Because the low-pressure argon gas was only 5 MPa, it could not penetrate into all the cavities. Thus, there are lots of cavities that are blocked in the green sample. A small portion of air was likely left in the cavities after mold pressure. With the temperature increasing, more and more H_2 decomposed from $TiH_{1.5}$. Furthermore, the volumes of the remaining air and the decomposed H_2 in the closed cavities would become more and more. The final sintering temperature is 1050 °C, which is above the eutectic temperature (942 °C) of Ni–Ti binary system. Therefore, liquid phase should appear in the specimen during sintering. In order to reduce the surface energy, the separate gas bubbles would merge together and form a larger one. This happen because a few sample pores remain in the sample III. The argon gas was released suddenly once the sintering was over. The pressure of the cavities is higher than the pressure out of the specimen. The gas trapped in the closed pores would expand at the same time. The closed pores expand in the soft medium because of the pressure difference across the pore wall. Some walls between two neighboring pores are much thinner, so the pores merge with each other when the adjacent walls are pierced during expansion. If one of the pores is an open one, the open porosity would be enlarged by the merged pore. If all the pores are closed ones, they would become larger than the pores before the merger. The merged pores are left in the sample all through until the furnace temperature was cooled down to room temperature. Some walls around the closed pores are too strong to be pierced during expansion. These pores would expand to larger spherical ones, which is favorable to the formation of porous structure with lower stress concentration around the pores.

Thus, porous NiTi SMAs with high porosity and large pore size can be formed by LPS when titanium hydride is introduced in the green samples. Li et al. [15] added TiH_2 to the original powder and fabricated porous NiTi SMAs by CS under vacuum environment. The decomposed H_2 would escape from the green sample due to vacuum. Thus, they reported that the pore size becomes smaller and the pore number increases with TiH_2 addition. It is suggested that the low gas pressure (5 MPa) is enough to prevent H_2 from being released from the green sample. Consequently, LPS is an effective method to produce porous NiTi SMAs with high porosity and large pore size using titanium hydride as the pore-forming agent.

Microstructure evaluation

Figure 3 shows the XRD patterns of the sintered samples using LPS with different porosities. It reveals that the use of $TiH_{1.5}$ can greatly affect the pore features but not the composition and phase constituent of the alloys. It is found that NiTi (B2) and NiTi (B19′) are the dominant phases in the samples prepared by LPS. The secondary phases such as Ti_2Ni and $TiNi_3$ were also found in all the samples. It is hard to obtain samples fully from the NiTi phase because of the narrow range of NiTi phase in the Ni–Ti binary phase diagram. The Gibbs free energies of NiTi, Ti_2Ni, and $TiNi_3$ indicate that the driving force for the formation of Ti_2Ni and $TiNi_3$ is stronger than that of NiTi [17]. Therefore, it is difficult to suppress the formation of the

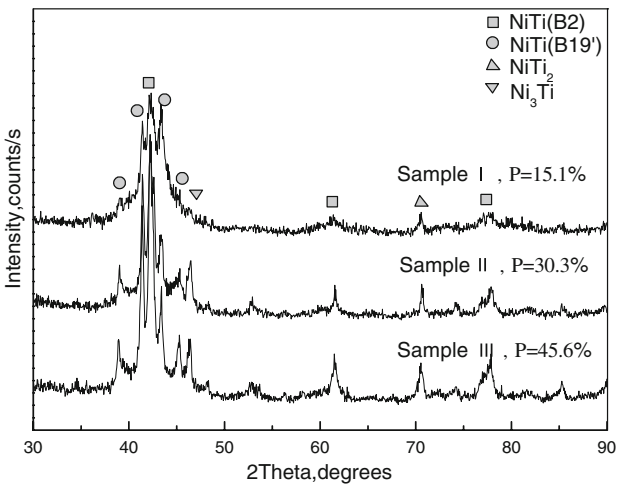

Fig. 3 XRD patterns of sintered samples prepared by LPS with different porosities

secondary phase such as Ti_2Ni and $TiNi_3$. This result is similar to those reported by others in the porous NiTi SMAs prepared by CF-HIP [18]. It may imply that the hot pressure has almost no influence on the phase constituent.

Martensitic transformation behavior analysis

Figures 4 and 5 show the DSC results of the porous Ti–50.8at.%Ni SMAs with different porosity ratios varying from 15.1% to 45.6%. In order to exactly determine the correlation between the phase transformation temperature and the porosity, the temperature at exothermic peaks were measured for the samples with different porosities.

It is worth while to note that aging can significantly influence the phase transformation behavior of porous NiTi SMAs. It can be seen from Figs. 4 and 5 that there is one peak in specimen without aging in heating and cooling curves. However, there is a multi-stage martensitic transformation (MST) that occured in the specimen after aging. It may be due to the extra internal stress introduced by Ni_4Ti_3 precipitation [18], which makes a direct transformation from B2 phase to B19′ phase more difficult after aging, because it needs more energy for the martensitic transformation. However, it needs less energy for R-phase transformation. So, the Ni_4Ti_3 precipitation favors the formation of R-phase.

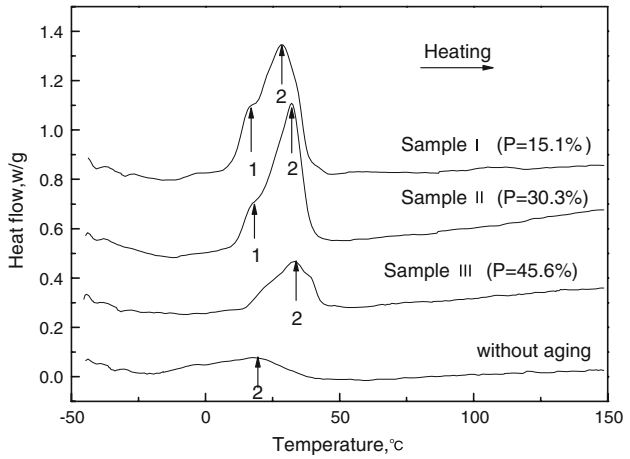

Fig. 4 DSC heating curves of the porous Ti–50.8at.%Ni SMAs prepared by LPS with different porosity ratios

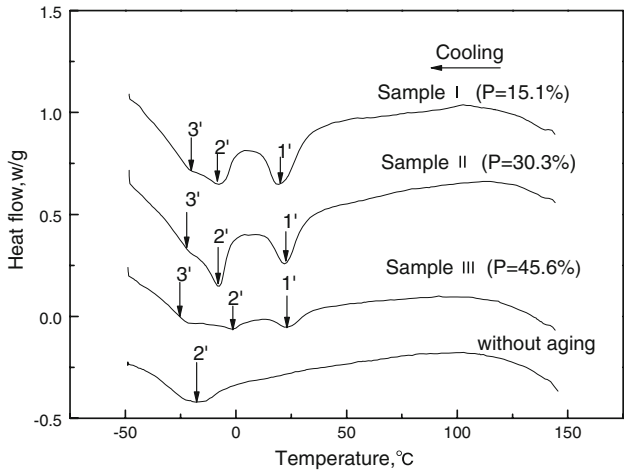

Fig. 5 DSC cooling curves of the porous Ti–50.8at.%Ni SMAs prepared by LPS with different porosity ratios

For the heating curves of the aged samples, it can be seen from Fig. 4 that a two-step phase transformation takes place during heating. With increasing porosity ratio, the superposition of the two endothermic peaks becomes more obvious. It is known that the peaks 1 and 2 in the heating curves correspond to the R-phase transformation and the B19′ martensitic transformation, respectively [19]. However, Su and Wu [20] reported that the peaks 1 and 2 in the heating curves correspond to B19′ → R → B2 and B19′ → B2, respectively.

A three-step transformation during cooling could be found in Fig. 5. The peak 1′ should correspond to the B2 → R transformation, the peak 2′ to the R → B19′ transformation, and the peak 3′ to the remaining R-phase to B19′ transformation [21]. Carroll et al. [22] believed that the transformation in the second step is not completely due to the obstacle of the dislocation. Moreover, it can be seen from Fig. 5 and Table 2 that the R-phase transformation changes slightly, while the M_f becomes lower with increasing porosity. Recently, Filip and Mazanec [23] reported that Ni_4Ti_3 particles primarily form at the grain boundaries in the supersaturated NiTi SMAs without defects. Allafi observed through TEM which showed that the Ni_4Ti_3 particles preferably precipitate at the domain of 2 μm near the grain boundary in the NiTi sample aged for short time [24], but there is no precipitation in the grain. Grain boundary (or other interfaces such as pore wall) can reduce the interface energy between the precipitation and the matrix. Hence, grain boundary can favor the nucleation and growth of the Ni_4Ti_3 particles [25, 26]. As for the porous NiTi SMAs, there do exist a lot of pores and these pore walls can be treated as an interface, which may play a similar role as the grain boundary. With the increasing porosity or pore surface area,

Table 2 Transformation temperatures of the porous Ti–50.8at.%Ni SMAs prepared by LPS with different porosities

Porosity	Transformation temperature (°C)				
	P1	P2	P1′	P2′	P3′
15.1%	17.0	28.4	20.0	−8.4	−20.3
30.3%	18.2	32.1	22.5	−7.9	−22.3
45.6%		33.7	22.5	−1.5	−25.4
Without aging		19.4		−17.8	

these pore walls are conducive to precipitating more and more Ni_4Ti_3 particles. The induced strain of B19′ martensitic transformation is 10 times that of the R-phase transformation. Hence, Ni_4Ti_3 precipitation has a stronger influence on the B19′ martensitic transformation.

Mechanical performance evaluation

Figure 6a–c shows the compressive stress–strain curves of the samples I–III. The comparison of compression behaviors of the porous TiNi SMAs prepared by different methods is shown in Table 3. It was revealed in Fig. 6a that sample I shows almost complete superelasticity after the second cycle. The plastic strain was only about 0.3% after two cycles training. The ultimate compressive strength of the sample I is up to 440 MPa. It can be seen from Table 3 that Zhao et al. [9] fabricated porous NiTi alloy with 13% porosity using SPS. The compression strength is 680 MPa when the compressive strain is up to 5%. In their study, the compression strength is about 480 MPa when the compressive strain is 4%. It is similar to that of the sample I. However, the powders used in SPS are pre-alloy NiTi powders, which complicated the manufacturing process compared with LPS.

Figure 6b and c shows the compressive stress–strain curves of the sample II and the sample III. It was revealed in Fig. 6b that the sample II shows almost complete superelasticity after the third cycle. The plastic strain was only about 0.3% after two cycles training. The ultimate compressive strength of the sample II is up to 340 MPa, which is higher than that of the compact human bone and can, therefore, meet the strength demand of hard tissue implants. However, the increase of porosity reduces the superelasticity. The sample III, which had higher porosity, exhibited partial superelasticity, the plastic strain of the sample III being about 1.6% after two cycles. It can be concluded that the porous NiTi SMAs with appropriate porosity prepared by LPS have sufficiently good mechanical properties and superelasticity after cycling. Moreover, porous NiTi SMAs with high porosity fabricated by using titanium hydride as the pore-forming agent also exhibit superelasticity. It can be seen from Fig. 6b and c that the elastic modulus and strength of the samples decrease with increasing porosity. It is due to the area of load-bearing in the sample with big pores and high porosity being smaller than that of the sample with small pores and low porosity. On the other hand, in the porous NiTi alloys with higher porosity, the quantity of austenite transformed into martensite per unit volume is less than that in the alloys with lower porosites. Hence, a lower critical stress can induce martensite transformation in the porous NiTi alloys with higher porosites. This result is similar to that of the porous NiTi SMAs prepared by CF-HIP [27]. The porous structure

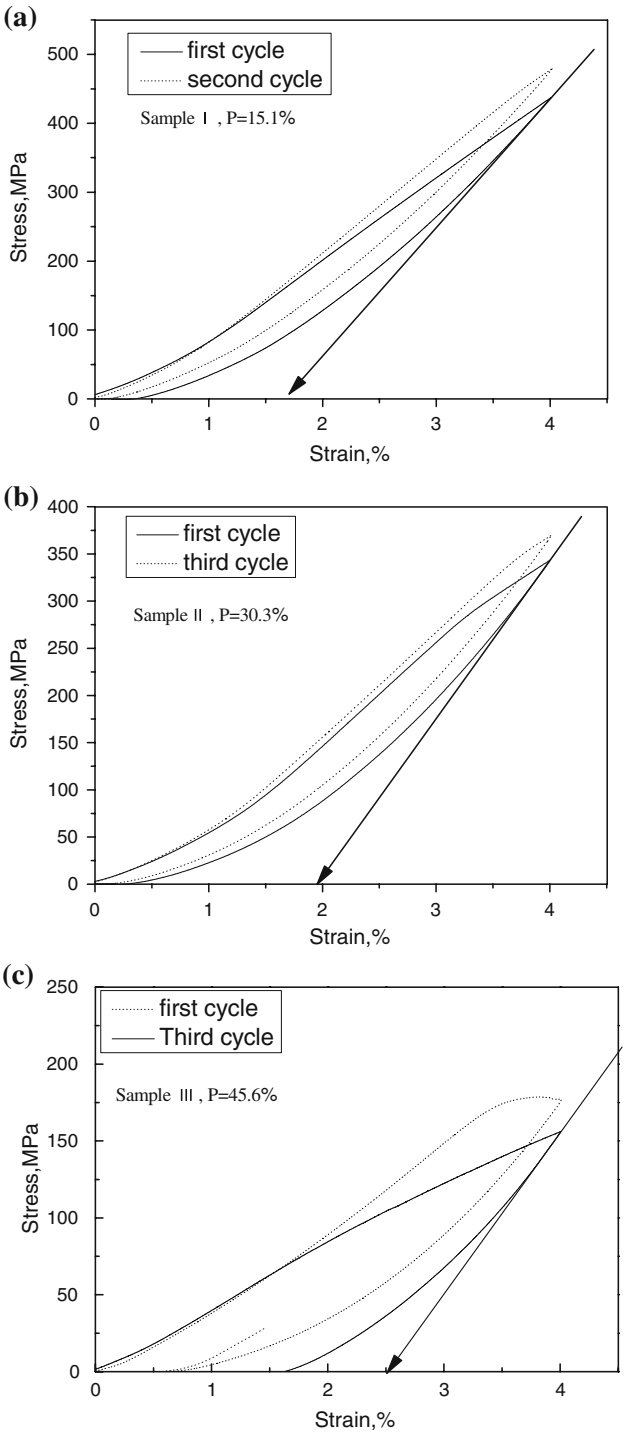

Fig. 6 Compressive stress–strain curves of porous NiTi SMAs prepared by LPS after aging at 723 K for 0.5 h: **a** sample I; **b** sample II; **c** sample III

and the properties of porous NiTi SMAs prepared by LPS are similar to those obtained by CF-HIP. However, the sintering pressure of LPS ($\leq$5 MPa) is far lower than that of CF-HIP ($\geq$100 MPa). Therefore, it can reduce the considerable fabricating cost considerably.

Table 3 Comparison of compression behaviors of the porous TiNi SMAs prepared by different methods

Ref.	Porosity (%)	Strain (%)	Stress (MPa)	Fabricating methods
[8]	13	5	680	SPS
[26]	36	4	340	CF-HIP
[26]	48	2.8	130	CF-HIP
This work	15.1	4	440	LPS
	30.3	4	340	LPS
	45.6	4	155	LPS
	33.2	4	175	CS

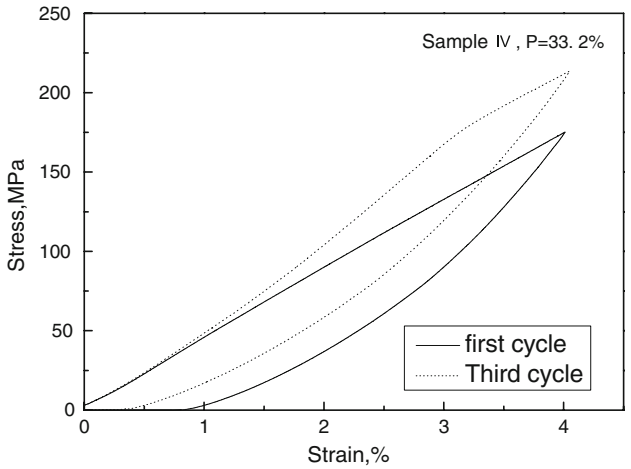

Fig. 7 Compressive stress–strain curve of porous NiTi SMAs prepared by CS after aging at 723 K for 0.5 h

Figure 7 shows the compressive stress–strain curve of the porous NiTi SMAs prepared by CS and aged at 450 °C for 0.5 h. The porosity of the specimen prepared by CS is similar to that of the sample II prepared by LPS. When the pre-strain of the porous NiTi SMAs is 4%, the plastic strain is about 0.8% after unloading, and the ultimate compressive strength of porous NiTi SMAs is up to 200 MPa. This result is superior to those reported by others for the porous NiTi SMAs prepared by CS [28]. However, it is not as good as the specimen with the same porosity prepared by LPS. This is due to the fact that the pore shape of the porous NiTi SMAs prepared by LPS is more spherical than that prepared by CS. Thus, the mechanical properties of the porous NiTi SMAs prepared by LPS are superior to that prepared by CS with the same porosity.

Conclusions

Porous Ti–50.8at.%Ni SMAs with high porosity and large pore size were successfully fabricated by LPS method using $TH_{1.5}$ as the pore-forming agent. The fabricated alloys exhibit nearly spherical pore and homogeneous porous distribution. By changing the cold compression pressure, original powder, and sintering pressure, the pore size of the porous NiTi SMA prepared by LPS can be controlled accordingly from 50 to 350 μm, and the porosity can be adjusted to vary from about 15% to 46%. The porous NiTi SMAs prepared by LPS exhibit good mechanical properties and superelasticity after thermo-mechanical cycling.

Acknowledgements The authors acknowledge the support from National Natural Science Foundation of China (No.50701019), China Postdoctoral Science Foundation (No. 20060390199), the Ministry of Education (Project No IRT0551), Guangdong Provincial Natural Science Foundation (2005 Team project), and City University of Hong Kong Grant (Project No.7002215).

References

1. Bansiddhi A, Sargeant TD, Stupp SI et al (2008) Acta Biomater 4:773
2. Zhao Y, Taya M, Izui H (2006) Int J Solid Struct 43:497
3. Zhou JB, Gao LP, Wang KS (2005) J Rare Earth 23:449
4. Levine B (2008) Adv Eng Mater 10:788
5. Green SM, Grant DM, Kelly NR (1997) Powder Metall 40:43
6. Li BY, Rong LJ, Li YY (1998) J Mater Res 13:2847
7. Otaguchi M, Kaieda Y, Oguro N (1990) J Japan Inst Metals 54:214
8. Li BY, Rong LJ, Li YY, Gjunter VE (2000) J Mater Res 15:10
9. Zhao Y, Taya M, Kang YS, Kawasaki A (2005) Acta Mater 53:337
10. Vandygriff EC, Lagoudas DC, Thangarai JK, Chen YC (2000) Proceedings of ASC 15th annual technical conference. Technomic Publishing Co Inc., Lancaster, p 239
11. Yuan B, Chung CY, Zhu M (2004) Mater Sci Eng A 382:181
12. Bansiddhi A, Dunand D (1612) Intermetallics 15:1612
13. Zhang YP, Yuan B, Zeng MQ, Chung CY, Zhang XP (2007) J Mater Process Technol 192:439
14. Yuan B, Zhu M, Gao Y, Chung CY (2008) Smart Mater Struct 17:025013
15. Li BY, Rong LJ, Li YY, Gjunter VE (2000) Metall Mater Trans A 31:1867
16. Ayers RA, Simske SJ, Bateman TA (1999) J Biomed Mater Res 45:42
17. Barin I (1989) Thermochemical data of pure substances. Weinheim, Federal Republic of Germany; VCH, New York
18. Bataillard L, Bidaux E, Gotthardt R (1998) Philos Magn 78:327
19. Miyazaki S, Otsuka K, Wayman CM (1989) Acta Metall 37:1873
20. Su PC, Wu SK (2004) Acta Mater 52:1117
21. Wu SL, Liu XM, Chu PK (2008) J Alloy Compd 449:139
22. Carroll MC, Somsen CH, Eggler G (2004) Scr Mater 50:187
23. Filip P, Mazanec K (2001) Scr Mater 45:701
24. Allafi JK, Dlouhy A, Eggeler G (2002) Acta Mater 50:4255
25. Porter DA, Easterling KE (1997) Phase transformations in metals and alloys. Reprinted 2nd edn. Chapman and Hall, London
26. Zhou YM, Zhang J, Fan GL et al (2005) Acta Mater 53:5365
27. Wu SL, Chung CY, Liu XM et al (2007) Acta Mater 55:3437
28. Li BY, Rong LJ, Li YY (2000) Intermetallics 8:643